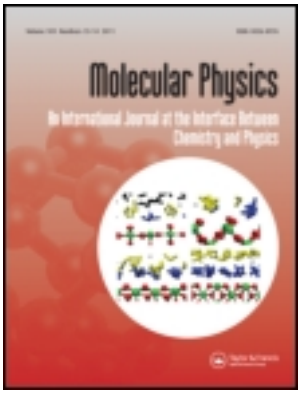

Molecular Physics: An International Journal at the Interface Between Chemistry and Physics
Publication details, including instructions for authors and subscription information:
http://www.tandfonline.com/loi/tmph20

Time reversal of cross-polarization in solid-state NMR

MATTHIAS ERNST , BEAT H. MEIER , MARCO TOMASELLI & ALEXANDER PINES

Version of record first published: 03 Jan 2012.

To cite this article: MATTHIAS ERNST , BEAT H. MEIER , MARCO TOMASELLI & ALEXANDER PINES (1998): Time reversal of cross-polarization in solid-state NMR, Molecular Physics: An International Journal at the Interface Between Chemistry and Physics, 95:5, 849-858

To link to this article: http://dx.doi.org/10.1080/002689798166477

MOLECULAR PHYSICS, 1998, VOL. 95, NO. 5, 849–858

Time reversal of cross-polarization in solid-state NMR

By MATTHIAS ERNST[1]†, BEAT H, MEIER[1]†, MARCO TOMASELLI[2] and ALEXANDER PINES[2]

[1] NSR-Center for Molecular Structure, Design, and Synthesis, Laboratory of Physical Chemistry, University of Nijmegen, Toernooiveld 1, NL-6525 ED Nijmegen, The Netherlands

[2] Materials Sciences Division, E. O. Lawrence Berkeley National Laboratory, 1 Cyclotron Road, Berkeley, CA 94720, and Department of Chemistry, University of California, Berkeley, California 94720, USA

(*Received 9 January 1998; accepted 25 February 1998*)

Cross-polarization at the Hartmann–Hahn condition in solid-state NMR frequently is described in terms of thermodynamics. Spin temperatures characterizing the canonical density operator are assigned to the Zeeman reservoirs of the two spins and the cross-polarization process brings about a state of equilibrium of the two reservoirs with a common temperature. In such a model, cross-polarization from an initially polarized spin species (I spins) to another spin species (S spins) is inherently an irreversible process accompanied by an increase in the entropy of the system. However, a cross-polarization echo can be generated whereby the polarization transferred to the S spins returns to the I spins, restoring the initial density operator. Therefore a thermodynamic description should be applied with care even in samples where the build-up and the decay of the magnetization can be approximated well by multi-exponential processes. Such cross-polarization echoes are formed by the consecutive application of two pulse trains that produce effective Hamiltonians differing in sign. The 'time reversal' of cross-polarization is consistent with both the increase in Zeeman entropy during the approach to equilibrium and with the constraint of unitary quantum evolution.

1. Introduction

Cross-polarization [1, 2] is a standard technique in solid-state nuclear magnetic resonance (NMR) spectroscopy and commonly is used to enhance the sensitivity of spins with low natural abundance and/or low magnetogyric ratio γ (S spins) by transferring polarization from abundant high-γ spins (I spins). Such experiments can also be used to determine the spatial neighbourhood of spin systems or to increase the repetition rate of experiments by exploiting differences in relaxation times. Cross-polarization relies on matching the amplitudes of the two radiofrequency (RF) fields B_{1I} and B_{1S} at the Hartmann–Hahn condition which for spin-1/2 nuclei is given by $|\omega_{1I}| = |\omega_{1S}|$ with $\omega_{1I} = -\gamma_I B_{1I}$ and $\omega_{1S} = -\gamma_S B_{1S}$. At the Hartmann–Hahn condition, the energy-level splitting of the I and S spins matches in the 'rotating frame', and energy-conserving flip-flop transitions are possible.

In a tilted doubly rotating frame with the z axis of the two spins aligned along the direction of the RF irradiation, the part of the heteronuclear dipole interaction that promotes the transfer of polarization between the two spin species is given by

$$\mathcal{H}_{IS} = \sum_{i,j} -\tfrac{1}{2}\omega_{IS}^{(i,j)} \cdot (I_i^+ S_j^- + I_j^- S_j^+), \qquad (1)$$

where i sums over all I spins, j sums over all S spins, and

$$\omega_{IS}^{(i,j)} = \frac{\mu_0}{4\pi}\frac{\gamma_I\gamma_S\hbar}{r_{ij}^3} P_2(\cos\theta_{ij}) \qquad (2)$$

denotes the orientation-dependent dipolar-coupling frequency between the spins i and j. Here, $P_2(\cos\theta_{ij})$ is the second-order Legendre polynomial [3], and θ_{ij} is the inclination angle of the internuclear vector with the static magnetic field.

In a two-spin system the Hamiltonian of equation (1) leads to an oscillatory polarization transfer between the two spins. The time evolution becomes more complicated in many-spin systems and in systems with homonuclear dipolar couplings [4]. In a dense coupling network, the time evolution of the cross-polarization process often is described by a thermodynamic model [5] where the I spin and the S spin 'baths' are each

† Present address: Laboratorium für Physikalische Chemie, ETH-Zentrum, CH-8092 Zürich, Switzerland.

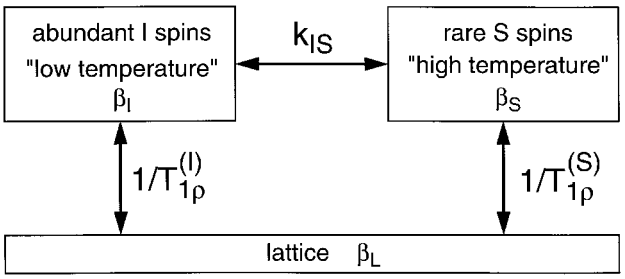

Figure 1. Thermodynamic model of Hartmann–Hahn cross-polarization. Two spin species are characterized by inverse spin temperatures β_I and β_S. The transfer of magnetization is described by three rate constants: k_{IS} describes the flow of magnetization between the I-spin and the S-spin reservoir while $1/T_{1\rho}^{(I)}$ and $1/T_{1\rho}^{(S)}$ describe the interaction of the spins with the lattice ($T_{1\rho}$ relaxation) which is at an inverse temperature β_L.

characterized by a single variable, the inverse spin temperature $\beta_R = \hbar/(k_B T_R)$. Here, k_B is the Boltzmann constant, and T_R is the temperature of the spin bath that characterizes the Boltzmann distribution of the populations. The inverse spin temperature of a reservoir is obtained from the quantum-mechanical density operator by a projection onto the reservoir Hamiltonian $\mathcal{H}_R$:

$$\beta_R = -\mathrm{Tr}\{1\}\frac{\langle \mathcal{H}_R|\sigma\rangle}{\langle \mathcal{H}_R|\mathcal{H}_R\rangle}. \qquad (3)$$

If the Hartmann–Hahn condition is fulfilled the reservoir Hamiltonians usually are identified with the Zeeman Hamiltonians of the two spin species. In the laboratory frame of reference we have $\mathcal{H}_I = \omega_0^{(I)}\sum_i I_{iz}$ and $\mathcal{H}_S = \omega_0^{(S)}\sum_i S_{iz}$, in the tilted doubly rotating frame $\mathcal{H}_I = \omega_{1I}\sum_i I_{iz}$ and $\mathcal{H}_S = \omega_{1S}\sum_i S_{iz}$. Obviously, β_R can be a good description of the spin state only if the coherences, i.e., the part of the density operator that does not commute with the reservoir Hamiltonian, are irrelevant because they decay quickly. This assumption underlies the so-called spin-temperature hypothesis [6].

In the simplest version of the thermodynamic model, one assumes two Zeeman energy reservoirs (in the tilted doubly rotating frame) for the two spin species at different initial inverse temperatures, $\beta_I^{\mathrm{initial}}$ and $\beta_S^{\mathrm{initial}}$ (figure 1). The two reservoirs are coupled to the lattice by rotating-frame relaxation which is characterized by the relaxation times of the two spin systems $T_{1\rho}^{(I)}$ and $T_{1\rho}^{(S)}$, and to each other by the cross-polarization process which is characterized by a single rate constant k_{IS}. Then the time evolution of the spin system can be described by a system of coupled differential equations for the inverse spin temperatures [5, 7]

$$\frac{\mathrm{d}}{\mathrm{d}t}\beta_S = -k_{IS}(\beta_S - \beta_I) - \frac{1}{T_{1\rho}^{(S)}}\beta_S,$$

$$\frac{\mathrm{d}}{\mathrm{d}t}\beta_I = -\varepsilon' k_{IS}(\beta_I - \beta_S) - \frac{1}{T_{1\rho}^{(I)}}\beta_I. \qquad (4)$$

For two spins with the same spin quantum number and at Hartmann–Hahn match, $\varepsilon' = N_S/N_I$ is the number of S spins per I spin and usually is a small number for systems with dilute S spins. During the cross-polarization process, polarization is exchanged between the initially strongly polarized I-spin reservoir (characterized by a low temperature) and the initially 'hot' S-spin reservoir until the two inverse temperatures in the doubly rotating frame reach equilibrium at $\beta_S^{\mathrm{final}} = \beta_I^{\mathrm{final}}$. The magnitude of the cross-polarization rate constant k_{IS} can be calculated from the crystal structure of the compound investigated and often agreement with experimental data is good [7, 8].

The entropy of the spin system characterized by a density operator σ is given by [5, 6]

$$S(t) = -k_B\,\mathrm{Tr}\{\tilde{\sigma}(t)\ln\tilde{\sigma}(t)\}, \qquad (5)$$

and is invariant under unitary transformations. Relaxation processes always lead to an increase in the entropy of the spin system. In the thermodynamic model of cross-polarization, only the Zeeman reservoirs of the density operator are considered. For an I–S spin, such a density operator $\tilde{\sigma}^Z(t)$ during the cross-polarization process can be described by

$$\tilde{\sigma}^Z(t) = \tfrac{1}{4}(1 - \beta_I(t)\mathcal{H}_I - \beta_S(t)\mathcal{H}_S). \qquad (6)$$

The entropy of the spin system described by such a density operator for a two-spin I–S system is given by

$$S(t) = k_B\left\{3\ln 2 - \tfrac{1}{8}\left[(\gamma_I B_{1I}\beta_I(t))^2 + (\gamma_S B_{1S}\beta_S(t))^2\right]\right\}, \qquad (7)$$

and is not constant during the cross-polarization process but increases monotonically. This increase is due to the fact that $S(t)$ depends on the sum of the squares of $\beta_I(t)$ and $\beta_S(t)$, which is minimum for $\beta_I(t) = \beta_S(t)$. Under the spin-temperature approximation, all components of $\tilde{\sigma}(t)$ not contained in $\tilde{\sigma}^Z(t)$ decay rapidly and can be neglected.

An indication that such a thermodynamic model is not always a good description of cross-polarization was the observation of 'transient oscillations' in the time dependence of cross-polarization in a single crystal of ferrocene [9]. Using the master equation approach of equation (4) in the framework of the thermodynamic model, such oscillations are not expected. They can, however, be explained by the presence of a dominant heteronuclear dipolar coupling between the S spins and one (or a few) of the I spins. The oscillations due

to this strong I–S dipolar coupling are damped by the interaction with all the other I spins. Such a situation can be described by considering the dominant I–S interaction quantum mechanically as an isolated two-spin system while still treating the rest of the interactions using the thermodynamic model of spin temperatures [9, 10].

Despite the fact that the master-equation approach of equation (4) frequently is capable of phenomenologically describing the cross-polarization process satisfactorily [5], cross-polarization is a deterministic unitary process that conserves quantum statistical entropy. The conservation of entropy is in contrast to the thermodynamic model in which entropy always increases. Since the entropy of the total density operator is constant under unitary rotations [5], it is obvious that the entropy of additional degrees of freedom (e.g., dipolar order) has to decrease during the cross-polarization process. The deterministic nature of the cross-polarization process can be demonstrated by stimulating an 'echo' that restores the initial quantum state of the system (e.g., all polarization localized on the protons) after cross-polarization has already proceeded substantially towards the equilibrium state.

The ability to manipulate the nuclear spin Hamiltonian has led to the observation of a large number of echo phenomena in NMR. The first spin echo [11] showed that it is possible to refocus inhomogeneously broadened lines by a single pulse. Later it was shown that it is also possible to refocus coherences in homonuclear dipolar-coupled many-spin systems [12, 13] by inverting the sign of the effective dipolar Hamiltonian of the system. Such a 'time reversal' of the free-induction decay (FID) can be achieved by combining the evolution in the absence of RF irradiation ('laboratory frame') with evolution under strong RF irradiation ('rotating frame') where the dipolar Hamiltonian has a different sign. The evolution under these two Hamiltonians leads to the so-called 'magic-echo', which demonstrated the first example of violation of the spin-temperature hypothesis [13]. The same principle has been exploited in order to refocus the spatial spread of initially localized polarization by creating a polarization echo [14]. An echo of the homonuclear spin-diffusion process under sample rotation has also been demonstrated [15] by reorienting the angle of the sample rotation axis using a dynamic-angle spinning (DAS) probe [16]. Echo experiments under magic-angle spinning also were described in the literature [17, 18], and a many-body echo was reported in zero-field NMR [19].

The echo experiments described above are all purely homonuclear experiments. In order to reverse the cross-polarization process and to obtain a cross-polarization echo, it is necesary to invert the full Hamiltonian, i.e., the heteronuclear dipolar Hamiltonian and both S-spin and I-spin homonuclear dipolar Hamiltonians, a situation considerably more demanding than that for purely homonuclear spin systems. From a theoretical viewpoint, however, the homonuclear polarization echo experiment and the cross-polarization echo experiment are closely related. The relevant parts of the dipolar Hamiltonian are very similar and will, therefore, lead to similar phenomena.

In this paper we show theoretically and experimentally that, by combining two Hartmann–Hahn cross-polarization experiments with different effective-field directions, it is possible to invert the full dipolar Hamiltonian and to manipulate the cross-polarization process such that a cross-polarization echo is obtained. The appearance of the echo demonstrates unambiguously the unitary quantum mechanical nature of the cross-polarization process. It should be emphasized that the term echo is understood in the sense that an initial state is restored and the magnetization returns to the source, i.e., the I spins. For an experiment that detects the S spins, the echo is manifested as a reduction in the detected magnetization.

2. Theory

We start our description from the high field truncated Hamiltonian in the usual doubly rotating frame [5] (rotating about the z axis with the I-spin and the S-spin Larmor frequencies, ω_{0I} and ω_{0S}):

$$\mathcal{H} = \mathcal{H}_{II} + \mathcal{H}_{SS} + \mathcal{H}_{IS} + \mathcal{H}_{I} + \mathcal{H}_{S} + \mathcal{H}_{RF}, \qquad (8)$$

which is valid for both the cross-polarization periods τ_1 and τ_2 of the experiment shown in figure 2. The first five terms on the RHS of equation (8) constitute the internal

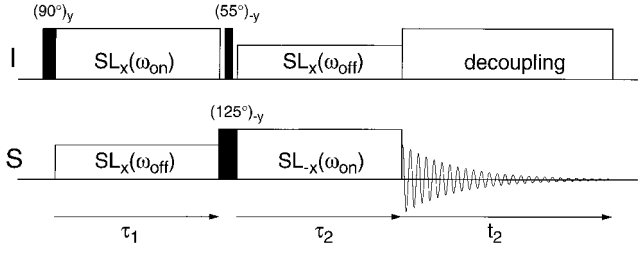

Figure 2. Pulse sequence used for the measurement of the cross-polarization echoes. After an initial 90° pulse, the I spins are irradiated on-resonance while the S spins are irradiated off-resonance such that the effective field is at an angle of $\theta_S = 35.26°$ with the static magnetic field. Both spins are then rotated into a new frame by a 55° I_y pulse and a 125° S_y pulse. In this new frame the S spins are irradiated on-resonance while the I spins are irradiated off-resonance such that the effective field is at an angle of $\theta_I = 35.26°$ with the static magnetic field. During the time t_2 the carbon signal is acquired under continuous-wave decoupling.

Hamiltonian and represent the homonuclear dipolar interactions of the I spins and the S spins, the heteronuclear dipolar interaction between the I spins and the S spins, and the chemical shifts of the I and S spins. They are defined as

$$\mathcal{H}_{\mathrm{II}} = \sum_{i<j} \omega_{\mathrm{II}}^{(i,j)} (3 I_{iz} I_{jz} - \mathbf{I}_i \cdot \mathbf{I}_j),$$

$$\mathcal{H}_{\mathrm{SS}} = \sum_{i<j} \omega_{\mathrm{SS}}^{(i,j)} (3 S_{iz} S_{jz} - \mathbf{S}_i \cdot \mathbf{S}_j),$$

$$\mathcal{H}_{\mathrm{IS}} = \sum_{i,j} \omega_{\mathrm{IS}}^{(i,j)} 2 I_{iz} S_{jz},$$

$$\mathcal{H}_{\mathrm{I}} = \sum_{i} \Omega_{\mathrm{I}}^{(i)} I_{iz},$$

$$\mathcal{H}_{\mathrm{S}} = \sum_{i} \Omega_{\mathrm{S}}^{(i)} S_{iz}. \qquad (9)$$

Here, $\omega_{\mathrm{II}}^{(i,j)}$ and $\omega_{\mathrm{SS}}^{(i,j)}$ are the homonuclear dipolar couplings among the I spins and the S spins, respectively. The heteronuclear dipolar couplings between the I spins and the S spins are given by $\omega_{\mathrm{IS}}^{(i,j)}$ and the chemical shifts (measured relative to $\omega_{0\mathrm{I}}$ and $\omega_{0\mathrm{S}}$, respectively) are described by $\Omega_I^{(i)}$ for the I spins and by $\Omega_{\mathrm{S}}^{(i)}$ for the S spins.

The last term of equation (8), the radiofrequency part of the Hamiltonian

$$\mathcal{H}_{\mathrm{RF}} = \omega_{1\mathrm{I}} F_{\mathrm{I}x} + \Delta_{\mathrm{I}} F_{\mathrm{I}z} + \omega_{1\mathrm{S}} F_{\mathrm{S}x} + \Delta_{\mathrm{S}} F_{\mathrm{S}z} \qquad (10)$$

contains the RF fields applied to the I spins and the S spins plus the RF carrier offset from $\omega_{0\mathrm{I}}$ or $\omega_{0\mathrm{S}}$ which differs from zero only during 'off-resonance' irradiation periods (figures 2 and 3). The $F_{i\alpha}$ denote total spin operators, e.g., $F_{ix} = \sum_i I_{ix}$; $\omega_{1\mathrm{I}}$ and $\omega_{1\mathrm{S}}$ describe the amplitudes of the I-spin and the S-spin RF irradiation, respectively; and Δ_{I} and Δ_{S} are the offsets of the RF irradiation frequency from $\omega_{0\mathrm{I}}$ and $\omega_{0\mathrm{S}}$.

We can now transform the Hamiltonian of equation (8) into a tilted frame [5, 20] such that the RF Hamiltonian and, therefore, the effective magnetic field direction, is aligned along the new z' axis. The tilted Hamiltonian is obtained by

$$\bar{\mathcal{H}} = U_{\mathrm{tilt}} \mathcal{H} U_{\mathrm{tilt}}^{\dagger}, \qquad (11)$$

with

$$U_{\mathrm{tilt}} = \exp\left[+\mathrm{i}(\theta_{\mathrm{I}} F_{\mathrm{I}y} + \theta_{\mathrm{S}} F_{\mathrm{S}y})\right] \qquad (12)$$

and

$$\theta_{\mathrm{I}} = \arctan\left(\frac{\omega_{1\mathrm{I}}}{\Delta_{\mathrm{I}}}\right) \quad \text{and} \quad \theta_{\mathrm{S}} = \arctan\left(\frac{\omega_{1\mathrm{S}}}{\Delta_{\mathrm{S}}}\right). \qquad (13)$$

In the next step, we remove the effective RF field term $\mathcal{H}_{\mathrm{RF}} = \omega_{\mathrm{I,eff}} F_{\mathrm{I}z} + \omega_{\mathrm{S,eff}} F_{\mathrm{S}z}$ from the tilted-frame Hamiltonian by transforming into an interaction-frame representation according to

$$\bar{\mathcal{H}}(t) = \exp(+\mathrm{i}\mathcal{H}_{\mathrm{RF}} t)\,\mathcal{H}\exp(-\mathrm{i}\mathcal{H}_{\mathrm{RF}} t). \qquad (14)$$

The effective field for the I spins is $\omega_{\mathrm{I,eff}} = (\Delta_{\mathrm{I}}^2 + \omega_{1\mathrm{I}}^2)^{1/2}$ and accordingly for the S spins $\omega_{\mathrm{S,eff}} = (\Delta_{\mathrm{S}}^2 + \omega_{1\mathrm{S}}^2)^{1/2}$. If the Hartmann–Hahn condition is fulfilled, i.e., $|\omega_{\mathrm{I,eff}}| = |\omega_{\mathrm{S,eff}}|$, the secular Hamiltonian that governs the time evolution of the spin system is given by

$$\begin{aligned}\bar{\mathcal{H}}_{\mathrm{sec}} = \bar{\mathcal{H}} = {} & P_2(\cos\theta_{\mathrm{I}})\mathcal{H}_{\mathrm{II}} + P_2(\cos\theta_{\mathrm{S}})\mathcal{H}_{\mathrm{SS}} \\ & + \cos\theta_{\mathrm{I}}\cos\theta_{\mathrm{S}}\mathcal{H}_{\mathrm{IS}} + \sin\theta_{\mathrm{I}}\sin\theta_{\mathrm{S}} \\ & \times \sum_{i,j} \omega_{\mathrm{IS}}^{(i,j)} (I_{\mathrm{ix}} S_{jx} + I_{iy} S_{jy}) \\ & + \cos\theta_{\mathrm{I}} \sum_i \Omega_{\mathrm{I}}^{(i)} I_{iz} + \cos\theta_{\mathrm{S}} \sum_i \Omega_{\mathrm{S}}^{(i)} S_{iz}. \end{aligned} \qquad (15)$$

Here, $P_2(\cos\theta) = (3\cos^2\theta - 1)/2$ is the second-order Legendre polynomial [3] and describes the truncation of a second-rank tensor under rotation about an axis inclined from the z axis by an angle θ.

In order to obtain a 'time reversal' of the time evolution of the density operator under this Hamiltonian and, therefore, a cross-polarization echo, it suffices to generate two interaction-frame Hamiltonians $\bar{\mathcal{H}}^{1)}$ and $\bar{\mathcal{H}}^{2)}$ during the two consecutive periods τ_1 and τ_2 of figure 2 that fulfil the relationship

$$\bar{\mathcal{H}}^{1)} = -\lambda \bar{\mathcal{H}}^{2)} \qquad (16)$$

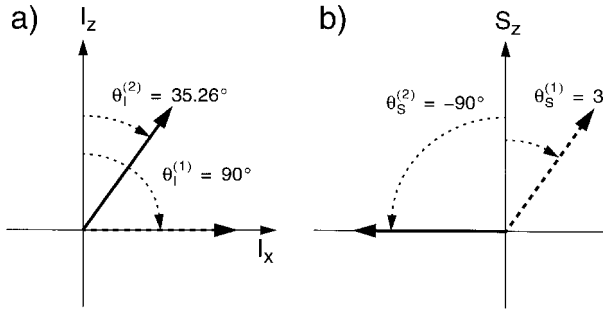

Figure 3. Orientations of the effective spin-lock fields in the xz plane used for the off-resonance Hartmann–Hahn experiments during the two time periods τ_1 and τ_2: (a) I spin; (b) S spin. The dashed arrows show the orientation of the effective spin-lock fields during the time period τ_1. The I spins are irradiated on-resonance while the S spins are irradiated such that the effective field is at an angle of $\theta_{\mathrm{S}}^{(1)} = 35.36°$ with the static magnetic field. The solid arrows show the orientation of the effective spin-lock fields during the time period τ_2. The S spins are irradiated on-resonance while the I spins are irradiated such that the effective field is at an angle of $\theta_{\mathrm{I}}^{(2)} = 35.26°$ with the static magnetic field.

where λ is a positive real number. The variables at the discretion of the experimentalist are the four angles $\theta_I^{(1)}$, $\theta_I^{(2)}$, $\theta_S^{(1)}$ and $\theta_S^{(2)}$. Furthermore, it is required that the density operator follows the changes in the quantization axis. Under these conditions, an echo will appear at $\tau_2 = \lambda\tau_1$. In the absence of chemical shift differences, where $\mathscr{H}_I$ and $\mathscr{H}_S$ vanish, solutions to equation (16) can be found by simultaneously solving the following four equations:

$$P_2(\cos\theta_I^{(1)}) = -\lambda P_2(\cos\theta_I^{(2)}), \tag{17}$$

$$P_2(\cos\theta_S^{(1)}) = -\lambda P_2(\cos\theta_S^{(2)}), \tag{18}$$

$$\cos\theta_I^{(1)}\cos\theta_S^{(1)} = -\lambda\cos\theta_I^{(2)}\cos\theta_S^{(2)}, \tag{19}$$

$$\sin\theta_I^{(1)}\sin\theta_S^{(1)} = -\lambda\sin\theta_I^{(2)}\sin\theta_S^{(2)}. \tag{20}$$

These four equations can only be solved simultaneously for $\lambda = 1$, i.e., if the two cross-polarization time periods have equal length. There exists an infinite set of solutions defined by:

$$35.26^\circ \geqslant \theta_I^{(1)} \geqslant 90^\circ,$$

$$\theta_I^{(2)} = \arccos\left[-\left(\frac{2-3\cos^2\theta_I^{(1)}}{3}\right)^{1/2}\right],$$

$$\theta_S^{(1)} = \arccos\left[\left(\frac{2-3\cos^2\theta_I^{(1)}}{3}\right)^{1/2}\right],$$

$$\theta_S^{(2)} = -\theta_I^{(1)}. \tag{21}$$

For the allowed range of angles $\theta_I^{(1)}$, the scaling factors for the homonuclear dipolar interaction (equations (17) and (18)) vary between +0.5 and −0.5 while the scaling factor for the heteronuclear dipolar interaction (equation (20)) varies between $1/3^{1/2}$ and 2/3. In the experiments, described below, we use the solution

$$\begin{aligned} \theta_I^{(1)} &= +90^\circ \qquad \theta_I^{(2)} = +35.26^\circ, \\ \theta_S^{(1)} &= +35.26^\circ \qquad \theta_S^{(2)} = -90^\circ, \end{aligned} \tag{22}$$

that leads to the scaling factors listed in table 1. It can be seen that all dipolar Hamiltonians change sign by going from the first cross-polarization time period (table 1, column 3) to the second time period (table 1, column 4). The chemical shift terms, however, are not inverted. They are scaled to zero during the on-resonance spin lock ($\theta = 90^\circ$) but only scaled by $(2/3)^{1/2}$ during the off-resonance spin lock ($\theta = 35.24^\circ$). This leads to an attenuation of the echo intensity unless the chemical shift offset and the chemical shielding tensors are very small. None of the solutions described by equation (21) leads to a simultaneous compensation of the two chemical shifts.

If only one of the two cross-polarization periods in figure 2 is active, we expect the same rate of polarization transfer irrespective of which of the two periods is chosen. This follows from the fact that the transferred magnetization is independent of the absolute sign of the Hamiltonian. However, the relaxation processes can differ for the two periods where the off-resonance spin lock is performed either on the S spins or on the I spins. In addition, the contributions from chemical shift offsets will be different in the two frames. Another source of imperfections that could inhibit full echo formation is incomplete truncation of the dipolar Hamiltonian by the effective RF field. If the effective RF field is not much larger than the line width of both the proton and carbon lines, the truncation applied in equation (15) is only approximately justified and higher order terms, not refocused by the echo scheme, would play a role.

3. Experimental implementation

An experimental implementation of the cross-polarization echo experiment using detection of the S spins (carbon) is shown in figure 2. After an initial 90° pulse, cross-polarization is allowed to proceed during the time period τ_1 with the I spins (protons) irradiated on-resonance while the S spins (carbons) are irradiated off-resonance to generate the required effective-field direction. Then a 55° pulse and a 125° pulse are applied simultaneously to the I spins (protons) and the S spins (carbons), respectively, in order to rotate the density operator into the new frame. During the time τ_2 the S spins (carbons) are irradiated on-resonance while the I spins (protons) are irradiated off-resonance (figure 3). The two times τ_1 and τ_2 can be varied independently to monitor the time dependence of the polarization transfer as a function of these two variables. In all cases, the carbon signal was acquired under continous-wave (CW) decoupling of the protons, and the intensity of the signal as a function of the two mixing times gives the two-dimensional echo envelope. As mentioned above, the cross-polarization echo manifests itself as a decay of the carbon magnetization. This pulse sequence can be used also to measure the time dependence of the build-up of the cross-polarized magnetization in each frame by setting one of the two times, τ_1 or τ_2, to zero. Spin-temperature alternation [21] was included in the phase cycle.

All experiments were carried out on a Chemagnetics CMX-180 spectrometer equipped with a 4 mm double-resonance MAS probe (used without sample spinning). Two differently selectively ^{13}C labelled samples, [2-^{13}C] glycine and [3-^{13}C] alanine, were used in the experiments. The effective field for the cross-polarization was in all

Table 1. Parameters for the cross-polarization echo experiment.

Parameters	On-resonance Hartmann–Hahn polarization	Off-resonance cross-polarization during τ_1	Off-resonance cross-polarization during τ_2
I-spin angle (θ_I)	90°	90°	35.26°
S-spin angle (θ_S)	90°	35.26°	-90°
Homonuclear I-spin scaling ($P_2(\cos\theta_I)$)	$-\frac{1}{2}$	$-\frac{1}{2}$	$+\frac{1}{2}$
Homonuclear S-spin scaling ($P_2(\cos\theta_I)$)	$-\frac{1}{2}$	$+\frac{1}{2}$	$-\frac{1}{2}$
Heteronuclear scaling ($\sin\theta_I \sin\theta_S$)	1	$-\frac{1}{\sqrt{3}}$	$+\frac{1}{\sqrt{3}}$
Heteronuclear scaling ($\cos\theta_I \cos\theta_S$)	0	0	0
I-spin chemical shift scaling ($\cos\theta_I$)	0	0	$+\sqrt{\frac{2}{3}}$
S-spin chemical shift scaling ($\cos\theta_S$)	0	$+\sqrt{\frac{2}{3}}$	0
I-spin RF field strength (ω_{1I})	γB_1	γB_1	$\frac{1}{\sqrt{3}}\gamma B_1$
S-spin RF field strength (ω_{1S})	γB_1	$\frac{1}{\sqrt{3}}\gamma B_1$	$-\gamma B_1$
I-spin offset frequency (Δ_I)	0	0	$+\sqrt{\frac{2}{3}}\gamma B_1$
S-spin offset frequency (Δ_S)	0	$+\sqrt{\frac{2}{3}}\gamma B_1$	0

experiments adjusted to $\omega_{I,eff}/(2\pi) = \omega_{S,eff}/(2\pi) = 100$ kHz. To achieve an effective field of $\omega_{eff}/(2\pi) = 100$ kHz for the off-resonance irradiation, the RF field strength was reduced to $\omega_1/(2\pi) \approx 57.7$ kHz. Off-resonance irradiation was generated either by a phase-continuous frequency jump of -81.650 kHz from the carrier frequency of the RF or by a continuous phase modulation of the on-resonance radiofrequency. In principle, both schemes are equivalent, but on our spectrometer the second method gave better and more reproducible results. For all experiments a completely filled 4 mm rotor was used. Phase errors due to changes in the probe tuning and matching as a function of RF frequency were compensated by experimentally adjusting the phase of the off-resonance irradiated radiofrequency field.

The RF field strengths on the two channels for the on- and off-resonance cross-polarization (CP) experiments were adjusted using the following four-step procedure.

(i) On-resonance cross-polarization. First the field strength on the proton channel was adjusted to approximately 100 kHz using a proton nutation experiment with cross-polarization and detection on the carbon channel. The RF amplitude of the carbon channel was then adjusted for optimum cross-polarization intensity and the field strength checked by a carbon nutation experiment. The difference in the nutation frequencies was less than 2%. The nutation spectra were fitted with a damped sine wave, and the extracted parameters were used to calculate the exact duration of the pulses required for the experiment (figure 2).

(ii) Carbon off-resonance cross-polarization. Using the CP echo pulse sequence (figure 2) with $\tau_2 = 0$ and the proton on-resonance field strength, the off-resonance cross-polarization condition for the carbon channel was optimized and the phase error carefully checked. Typically, the phase difference between the on-resonance and the off-resonance irradiation was less than 10°.

(iii) Proton off-resonance cross-polarization. The same adjustment was carried out to optimize the proton off-resonance RF field strength using the CP echo pulse sequence of figure 2 with $\tau_1 = 0$.

(iv) Fine tuning of the parameters. In a final step the off-resonance field strengths were fine tuned to give the lowest carbon intensity for $\tau_1 = \tau_2 \approx 100\,\mu$s and equal intensity for the build-up of the cross-polarized magnetization in the two different frames. Only very small adjustments of the RF field strength were necessary.

During the course of the measurements, it was noted that the experiment is rather sensitive to small misadjustments of the parameters. The misadjustments do not lead to a shift of the echo in time, as is the case for homonuclear dipolar echoes [12–15, 18], but to a decrease in the extent of the refocusing. This is a conse-

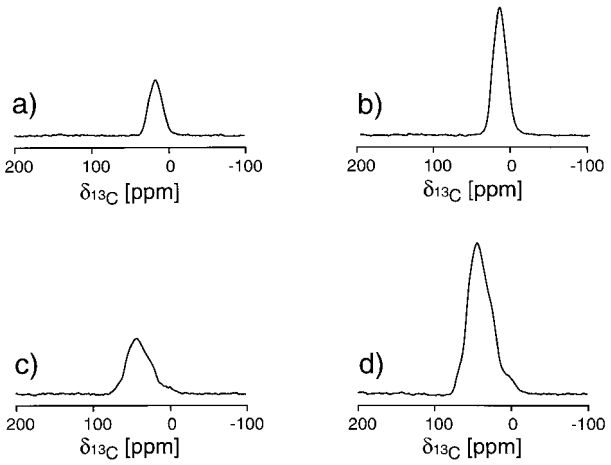

Figure 4. (*a*) One-pulse excitation carbon spectrum and (*b*) cross-polarization carbon spectrum of [3-^{13}C]alanine; (*c*) one-pulse excitation carbon spectrum and (*d*) cross-polarization carbon spectrum of [2-^{13}C]glycine. The chemical shifts are referenced to an external secondary standard of TMS. The cross-polarization intensities in figures 5–8 are all normalized such that the one-pulse excitation carbon spectra have unit intensity.

quence of the fact that the misadjustment of one parameter will scale various components of the dipolar Hamiltonian differently, preventing complete echo formation.

4. Results

Figure 4 shows the one-pulse excitation carbon spectra of (*a*) [3-^{13}C]alanine and (*c*) [2-^{13}C]glycine plus (*b*,*d*) cross-polarization carbon spectra of both samples to illustrate the signal-to-noise ratio obtained in the cross-polarization echo measurements. The line shape is dominated by the ^{13}C chemical shift anisotropy. All spectra were acquired with 8 scans and a spectral width of 25 kHz. The one-pulse excitation carbon spectra of figure 4(*a*,*c*) were used to normalize the intensity of all the cross-polarization echo measurements.

Figure 5 shows the build-up of the cross-polarized magnetization for a sample of [3-^{13}C]alanine for the case of on-resonance Hartmann–Hahn cross-polarization (○), for the case of carbon off-resonance irradiation with $\theta_S = 35.26^\circ$ (□), and for the case of proton off-resonance irradiation with $\theta_I = 35.26^\circ$ (◇). The signal intensities are normalized to the one-pulse carbon spectrum of figure 4(*a*). The on-resonance Hartmann–Hahn cross-polarization reaches a maximum of 2.3 for $\tau_{CP} \approx 0.45$ ms. Using the thermodynamic model for cross-polarization and taking into account the number of I and S spins, a theoretical polarization of 3.0 would be expected in the absence of $T_{1\rho}$ relaxation (taking into account only the directly bound protons).

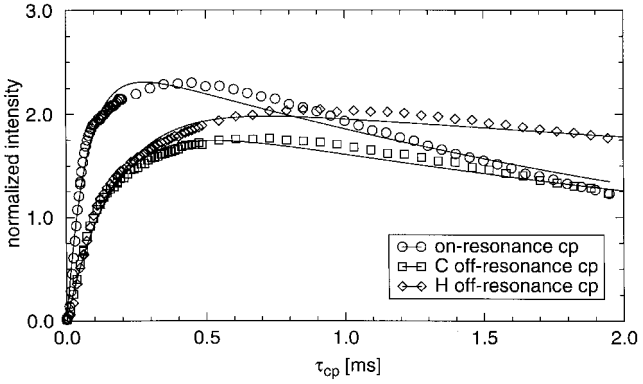

Figure 5. Time dependence of the build-up of the cross-polarized magnetization in [3-^{13}C]alanine. The build-up for the on-resonance Hartmann–Hahn cross-polarization is marked by a ○ while the solid lines show the best fit by the thermodynamic spin-temperature model (k_{IS} = 10 ms^{-1}). The build-up of the magnetization during the time period τ_1 (carbon irradiation off-resonance) is marked by □ and the build-up during the time period τ_2 (proton irradiation off-resonance) is marked by the symbol ◇. Again, the solid lines show the best fit by the thermodynamic spin-temperature model (k_{IS} = 4.5 ms^{-1} and 4.2 ms^{-1}, respectively). The signal intensity is normalized such that a comparable carbon one-pulse excitation spectrum has unit intensity.

Considering relaxation and instrumental imperfections (misadjustment of the Hartmann–Hahn match, miscalibration of the pulse lengths) the value obtained experimentally is quite reasonable. The carbon polarization build-up rate constant in the two different off-resonance frames is, as expected, slower than in the on-resonance Hartmann–Hahn case (figure 5) with fitted initial rate constants of 4.5 ms^{-1} for the off-resonance cross-polarization and 10 ms^{-1} for the Hartmann–Hahn case. The ratio of the two is reasonably close to the square of the scaling factor of the heteronuclear dipolar interaction [5] which is three (table 1). The solid lines in figure 5 show the best fits obtained by the thermodynamical model described in section 1. The agreement between the fitted curves and the measured data is less than perfect but still reasonable. This illustrates that the thermodynamic spin-temperature model agrees roughly with the measured data in this case. During the first 200 μs the time evolution of the cross-polarized magnetization is basically the same for the proton and the carbon off-resonance cross-polarization processes. For longer times the time evolution in the two off-resonance frames starts to deviate considerably, which is not accounted for by the simplified theoretical description.

In contrast to the cross-polarization build-up curve in alanine, which is roughly exponential, the data for [2-^{13}C]glycine shows pronounced transient oscillations [9], particularly strong in the on-resonance cross-polar-

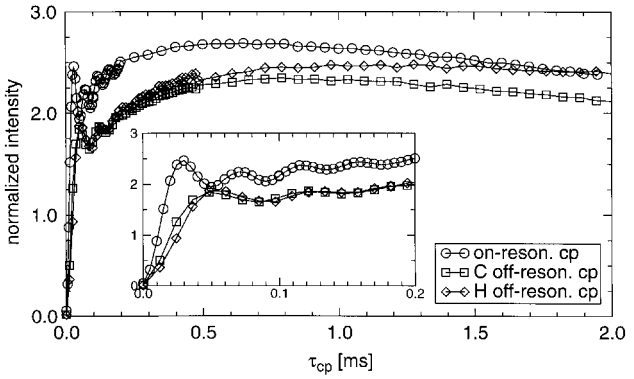

Figure 6. Time dependence of the build-up of the cross-polarized magnetization in [2-^{13}C]glycine. The build-up for the on-resonance Hartmann–Hahn cross-polarization is marked by a ○. The build-up of the magnetization during the time period τ_1 (carbon irradiation off-resonance) is marked by □ and the build-up during the time period τ_2 (proton irradiation off-resonance) is marked by the symbol ◇. The solid lines connect the measured data points as a guide to the eye. The inset shows a more detailed view of the curve for $\tau_{CP} < 200\,\mu s$. Transient oscillations of the cross-polaized magnetization are evident. The intensity is normalized such that a comparable carbon one-pulse excitation spectrum has unit intensity.

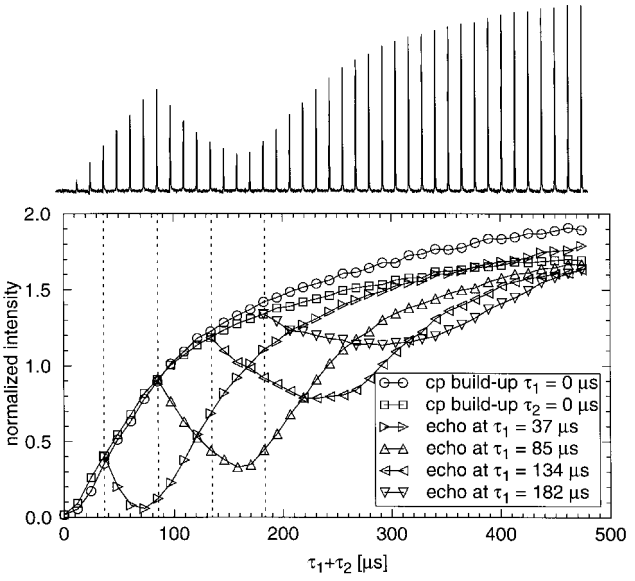

Figure 7. Cross-polarization echoes in [3-^{13}C]alanine. The build-up of the cross-polarized magnetization (see also figure 5) is shown for $\tau_1 = 0\,\mu s$ and $\tau_2 = 0\,\mu s$ marked with the symbols ○ and □, respectively. The data points marked with the symbols ▷, △, ◁, and ▽ represent the time evolution of the cross-polarized magnetization when the frame of the cross-polarization process is changed at time $\tau_1 = 37\,\mu s$, $85\,\mu s$, $134\,\mu s$, and $182\,\mu s$, respectively. These times are indicated in the figure by a dashed vertical line. The echoes are clearly visible at about the correct time point with $\tau_1 = \tau_2$, but for longer echo times τ_1 the minimum appears slightly earlier. The intensity of the minimum increases with increasing echo time. The solid lines connect the measured data points and are a guide to the eye. The upper part shows the actual spectrum for the echo formation when $\tau_1 = 85\,\mu s$.

ization measurements (figure 6). The oscillations are attributed to the strong heteronuclear coupling within the CH_2 group which exceeds the homogeneous proton line width. These transient oscillations are somewhat damped in both off-resonance cross-polarization cases because the heteronuclear interaction is scaled more strongly than the homonuclear interactions (table 1). The maximum magnetization of 2.7 times that of the one-pulse carbon spectrum (figure 4(*c*)) is reached after a mixing time of about 600 μs. The initial rate constants are $104\,ms^{-1}$ for on-resonance cross polarization and $45\,ms^{-1}$ for both off-resonance cross-polarization experiments. It is obvious that a purely thermodynamic model cannot accurately describe the cross-polarization process in this sample.

The formation of the echo in the [3-^{13}C]alanine sample for different echo times is shown in figure 7. The build-up of the cross-polarized magnetization in the two different frames is marked by the symbols ○ ($\tau_1 = 0\,\mu s$) and □ ($\tau_2 = 0\,\mu s$). These two curves are almost identical up to a cross-polarization time of 150 μs, after which they start to deviate slightly. The maximum intensity difference between the two curves for a cross-polarization time of 500 μs is about 10%. Four different echo experiments are shown in figure 7 and marked with the symbols ▷ for $\tau_1 = 37\,\mu s$, △ for $\tau_1 = 85\,\mu s$, ◁ for $\tau_1 = 134\,\mu s$, and ▽ for $\tau_1 = 182\,\mu s$. The series of ^{13}C spectra that corresponds to the echo curve with $\tau_1 = 85\,\mu s$ (△) is shown on top to illustrate the quality of the measured spectra. The small phase twists seen in some of the echo spectra were reproducible and their source is not fully understood. One possible cause is systematic phase errors generated by the limited phase resolution of the pulse programmer. The echo (signal minimum) reaches almost zero (the theoretically expected value corresponding to a perfect time reversal) for the shortest echo time, while for longer times the time reversal is not as good. This shows that the two effective Hamiltonians do not obey equation (16) precisely, due to experimental imperfections and true dissipative processes.

One possible source of the imperfections in the echo is the differences in the truncation of the chemical shift offsets or chemical shift tensors in the two different frames. Differences between the two Hamiltonians will lead to a different time evolution of the density operator, and therefore to an attenuation of the echo intensity. Other possible sources include misadjustments of the phase of the off-resonance RF field, the angle θ between

the effective field and the static magnetic field B_0, the pulse length for the rotation of the density operator from the first into the second frame, or of the Hartmann–Hahn match, i.e., the magnitude of the two effective fields. All these parameters were optimized experimentally as elaborated above for an echo time of 100 μs. However, there is always an unavoidable small drift of the linear amplifiers over the course of an experimental series, due to variations in environment parameters. Relaxation processes are also active during the cross-polarization time, as can be seen from the decay of the magnetization over longer contact times. Such an incoherent process destroys some of the coherences built up during the first cross-polarization interval τ_1. These coherences are therefore not completely refocused during the second cross-polarization interval τ_2, leading to an attenuated echo. Echoes are still observable up to an echo time of $\tau_1 \approx 200$ μs, but the intensity decays and they appear earlier than predicted.

Figure 8 shows the formation of cross-polarization echoes for [2-^{13}C]glycine for three different echo times τ_1. The shortest time, $\tau_1 = 37$ μs (figure 8(*a*)), is still in the very steep build-up regime of the cross-polarization process. The echo reaches almost zero intensity at the expected time τ_2. The second echo (figure 8(*b*)) with $\tau_1 = 85$ μs starts after the first transient oscillation reaches its minimum. It is interesting to see that the transient oscillation shows up also in the echo, as expected for a true time reversal. The carbon magnetization initially increases and after reaching a local maximum decreases, as expected, to form the echo. The echo at $\tau_1 = \tau_2$ is not complete (zero carbon intensity) but a value of about 50% of the maximum carbon signal amplitude is found. For the longest echo time with $\tau_1 = 134$ μs (figure 8(*c*)), the echo is considerably damped (higher carbon intensity at $\tau_1 = \tau_2$) compared with shorter echo times.

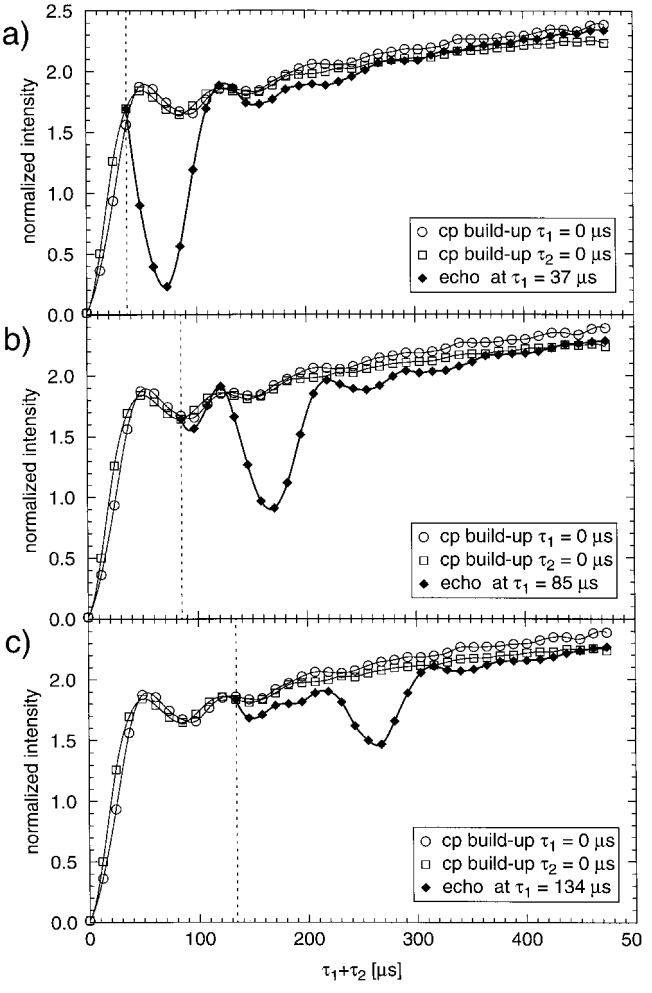

Figure 8. Cross-polarization echoes in [2-^{13}C]glycine. The build-up of the cross-polarized magnetization (see also figure 6) is shown for $\tau_1 = 0$ μs and $\tau_2 = 0$ μs marked with the symbols ○ and □, respectively. The data points marked with the symbols ◆ represent the time evolution of the cross-polarized magnetization when the frame of the cross-polarization process is changed at time (*a*) $\tau_1 = 37$ μs, (*b*) $\tau_1 = 85$ μs, and (*c*) $\tau_1 = 134$ μs. The echoes are clearly visible at about the correct time point with $\tau_1 = \tau_2$ but for longer echo times τ_1 the minimum appears slightly too early. The intensity of the minimum increases with increasing echo time. In (*b*) it can be seen that the transient oscillation appearing around $\tau_1 = 85$ μs is also time reversed. The solid lines connect the measured data points and are a guide to the eye.

5. Conclusion

Cross-polarization echoes were observed in static powder samples. The echo is obtained by a combination of two cross-polarization periods with different off-resonance RF irradiation schemes. The total (homonuclear and heteronuclear) dipolar interaction is the same during the two cross-polarization time periods, except for the sign of the Hamiltonian which is inverted during the second time period. The two different cross-polarization time periods correspond to different double tilted rotating frames.

The appearance of the echo confirms that cross-polarization is a coherent, unitary quantum mechanical process, despite the fact that in many cases it can be described approximately by a thermodynamic model with a master equation. In the experiments performed on the sample of alanine the observation of an almost exponential buildup and decay of the cross-polarization does not imply an incoherent heteronuclear relaxation process, reminding us that the spin-temperature hypothesis must be applied with care.

In contrast to the standard model of cross-polarization, where it is assumed that cross-polarization conserves the sum polarization and maximizes entropy, we deal with a process that conserves polarization as well as

total entropy of the spin system. Note that during the first of the cross-polarization periods the entropy increases if one considers only the Zeeman order of the two spin species, but the entropy of the additional degrees of freedom (dipolar order) decreases. During the second cross-polarization period, the Zeeman entropy decreases while the dipolar entropy increases. However, in the absence of $T_{1\rho}$ relaxation the total entropy of the density operator is constant, due to the conservation of entropy under unitary transformations. In the presence of relaxation, the entropy increases monotonically.

Dedicated to Prof. R. R. Ernst on the occasion of his 65th birthday.

Financial support from SON and the SON National HF-NMR Facility, University of Nijmegen, technical support by J. van Os, H. Janssen and G. Nachtegaal and stimulating scientific discussions with Rene Verel and Dr Paul Hodgkinson are gratefully acknowledged. We would also like to thank Dr Susan M. De Paul for many helpful suggestions and for carefully reading the manuscript. This work was supported by the Director, Office of Energy Research, Office of Basic Energy Sciences, Materials Sciences Division, US Department of Energy, under Contract DE-AC03-76SF0098.

References

[1] Hartmann, S. R., and Hahn, E. L., 1962, *Phys. Rev.*, **128,** 2042.
[2] Pines, A., Gibby, M. G., and Waugh, J. S., 1973, *J. chem. Phys.*, **59,** 569.
[3] Brink, D. M., and Satchler, G. R., 1993, *Angular Momentum* (Oxford: Clarendon Press).
[4] Meier, B. H., 1994, *Advances in Magnetic and Optical Resonance*, Vol. 18, edited by W. S. Warren (New York: Academic Press), p. 1.
[5] Mehring, M., 1983, *Principles of High Resolution NMR in Solids* (Berlin: Springer-Verlag).
[6] Goldman, M., 1970, *Spin Temperature and Nuclear Magnetic Resonance in Solids* (Oxford: Clarendon Press).
[7] McArthur, D. A., Hahn, E. L., and Walstedt, R. E., 1969, *Phys. Rev.*, **188,** 609.
[8] Demco, D. E., Tegenfeldt, J., and Waugh, J. S., 1975, *Phys. Rev.* B, **11,** 4133.
[9] Müller, L., Kumar, A., Baumann, T., and Ernst, R. R., 1974, *Phys. Rev. Lett.*, **32,** 1402.
[10] Levitt, M. H., Suter, D., and Ernst, R. R., 1986, *J. chem. Phys.*, **84,** 4243.
[11] Hahn, E. L., 1950, *Phys. Rev.*, **80,** 580.
[12] Schneider, H., and Schmiedel, H., 1969, *Phys. Lett.* A, **30,** 298.
[13] Rhim, W. K., Pines, A., and Waugh, J. S., 1970, *Phys. Rev. Lett.*, **25,** 218.
[14] Zhang, S., Meier, B. H., and Ernst, R. R., 1992, *Phys. Rev. Lett.*, **69,** 2149.
[15] De Paul, S. M., Tomaselli, M., Pines, A., Ernst, M., and Meier, B. H., 1997, *J. chem. Phys.*, **108,** 826.
[16] Mueller, K. T., Sun, B. Q., Chingas, G. C., Zwanziger, J. W., Terao, T., and Pines, A., 1990, *J. magn. Reson.*, **86,** 470.
[17] Karlsson, T., Helmle, M., Kurur, N. D., and Levitt, M. H., 1995, *Chem. Phys. Lett.*, **247,** 534.
[18] Tomaselli, M., Hediger, S. Suter, D., and Ernst, R. R., 1996, *J. chem. Phys.*, **105,** 10 672.
[19] Llor, A., Olejniczak, Z., Sachleben, J., and Pines, A., 1991, *Phys. Rev. Lett.*, **67,** 1989.
[20] Haeberlen, U., 1968, *High Resolution NMR in Solids: Selective Averaging* (New York: Academic Press).
[21] Stejskal, E. O., and Schaefer, J., 1975, *J. magn. Reson.*, **18,** 560.